

Molecular Dynamics Simulations of Water Permeation Across Nafion Membrane Interfaces

Kevin Brendan Daly, Jay B Benziger, Athanassios Z. Panagiotopoulos, and Pablo G. Debenedetti

J. Phys. Chem. B, Just Accepted Manuscript • DOI: 10.1021/jp5024718 • Publication Date (Web): 27 Jun 2014

Downloaded from <http://pubs.acs.org> on July 3, 2014

Just Accepted

"Just Accepted" manuscripts have been peer-reviewed and accepted for publication. They are posted online prior to technical editing, formatting for publication and author proofing. The American Chemical Society provides "Just Accepted" as a free service to the research community to expedite the dissemination of scientific material as soon as possible after acceptance. "Just Accepted" manuscripts appear in full in PDF format accompanied by an HTML abstract. "Just Accepted" manuscripts have been fully peer reviewed, but should not be considered the official version of record. They are accessible to all readers and citable by the Digital Object Identifier (DOI®). "Just Accepted" is an optional service offered to authors. Therefore, the "Just Accepted" Web site may not include all articles that will be published in the journal. After a manuscript is technically edited and formatted, it will be removed from the "Just Accepted" Web site and published as an ASAP article. Note that technical editing may introduce minor changes to the manuscript text and/or graphics which could affect content, and all legal disclaimers and ethical guidelines that apply to the journal pertain. ACS cannot be held responsible for errors or consequences arising from the use of information contained in these "Just Accepted" manuscripts.



ACS Publications

High quality. High impact.

The Journal of Physical Chemistry B is published by the American Chemical Society.

1155 Sixteenth Street N.W., Washington, DC 20036

Published by American Chemical Society. Copyright © American Chemical Society.

However, no copyright claim is made to original U.S. Government works, or works produced by employees of any Commonwealth realm Crown government in the course of their duties.

1
2
3
4
5
6
7
8
9
10
11
12
13
14
15
16
17
18
19
20
21
22
23
24
25
26
27
28
29
30
31
32
33
34
35
36
37
38
39
40
41
42
43
44
45
46
47
48
49
50
51
52
53
54
55
56
57
58
59
60

Molecular Dynamics Simulations of Water Permeation across Nafion Membrane Interfaces

Kevin B. Daly, Jay B. Benziger, Athanassios Z. Panagiotopoulos, and Pablo G.

Debenedetti*

Department of Chemical and Biological Engineering, Princeton University, Princeton, New Jersey 08544

E-mail: pdebene@princeton.edu

*To whom correspondence should be addressed

Abstract

Permeation of water across the membrane/vapor and membrane/liquid-water interfaces of Nafion is studied using non-equilibrium molecular dynamics (NEMD) simulations, providing direct calculations of mass transfer resistance. Water mass transfer within one nanometer of the vapor interface is shown to be two orders of magnitude slower than at any other point within the membrane, in qualitative agreement with permeation experiments. This interfacial resistance is much stronger than the resistance suggested by prior simulation work calculating self-diffusivity near the interface. The key difference between the prior approach and the NEMD approach is that the NEMD approach implicitly incorporates changes in solubility in the direction normal to the interface. Water is shown to be very insoluble near the vapor interface, which is rich in hydrophobic perfluorocarbon chains, in agreement with advancing contact angle experiments. Hydrophilic side chains are buried beneath this hydrophobic layer and aligned toward the interior of the membrane. Hydrophilic pores are not exposed to the vapor interface as proposed in prior theoretical work. At the membrane/liquid-water interface, highly swollen polymer chains extend into the liquid water phase, forming a nanoscopically rough interface that is consistent with AFM experiments. In these swollen conformations, hydrophilic side-chains are exposed to the liquid water phase, suggesting that the interface is hydrophilic, in agreement with receding contact angle experiments. The mass transfer resistance of this interface is negligible compared to that of the bulk, in qualitative agreement with permeation experiments. The water activity at the vapor and liquid-water interfaces are nearly the same, yet large conformational and transport differences are observed, consistent with a mass-transfer based understanding of Schroeder's paradox for Nafion.

Keywords: Nafion, ionomers, permeation, interfacial mass transfer

1 Introduction

Sulfonated, random copolymers constitute an extremely versatile class of permselective membranes with applications ranging from water purification¹ to chlor-alkali cells² to hydrogen fuel cells.³ As hydrogen fuel cell membranes, these polymers must be able to conduct protons while blocking the passage of anions. High proton conductivity for these polymers typically requires high humidity, since water molecules cluster around sulfonic acid groups to form a long-range network of proton donors and acceptors. As an example, the proton conductivity of the most widely used fuel cell membrane, Nafion,⁴ increases by four orders of magnitude if the humidity (water activity) is increased from 0% to 10%.⁵ The importance of water for proton conduction continues to motivate new research into water sorption, distribution, and transport in fuel cell membranes.^{6–9}

Given the strong coupling between proton conductivity and water activity ($a_w = f_w/f_w^{sat}$, where f_w is the fugacity of water and superscript “sat” denotes saturation conditions at the same temperature), it is tempting to humidify the feeds to the fuel cell in order to ensure adequate hydration of the membrane. Although this is indeed a common practice,¹⁰ it comes with a significant disadvantage: condensation of water in the flow channels. Liquid water hinders mass transfer of fuel to the catalyst, and must be pushed out of the gas flow channels by imposing a high gas flow rate,¹⁰ which in turn leads to a very low single pass conversion of fuel.¹¹

Fortunately, fuel conversion need not be compromised to achieve high membrane conductivity, as recent experimental work has shown.^{8,12–15} Water permeation, MRI, and X-ray microtomography measurements indicate that the membrane/vapor interface is a significant barrier to water mass transfer.^{8,12–15} In fact, if the membrane is exposed to water vapor on one side, and liquid water on the other, then the water mass transfer resistance of the vapor interface completely overwhelms the diffusional resistance for water transport across the membrane.^{12,13} This observation implies that the water activity profile starting from the liquid interface is relatively flat throughout the membrane, and then drops steeply at the membrane/vapor interface. This hypothesis appears to be supported by MRI measurements that exhibit a relatively flat signal intensity across interior of the membrane.¹⁵ Therefore, even if the anode side of a fuel cell is kept relatively dry, the water

activity *inside* the membrane can still be near saturation, provided that liquid water is present at the cathode. Liquid water at the cathode could be achieved without extra humidification because water is being produced there electrochemically.¹¹

Intriguingly, although the anode interface drastically impedes water transport, it appears to have a much more modest effect on proton transport. For example, Pivovar and Kim found that the membrane/electrode contact resistance for protons was approximately 10% of the overall resistance for a 100- μm thick Nafion membrane.¹⁶ Therefore, the interfacial properties of Nafion can be regarded as a critical advantage for fuel cell operation, and should be at least matched by any competing ionomer material. Currently, it is not obvious what chemical architecture an ionomer should have in order to replicate the interfacial properties of Nafion. Molecular simulations can improve understanding of structure-property relationships, since they provide molecular-level resolution while assuming very little about self-assembly of the membrane.

The interfacial properties of Nafion are also of fundamental interest, since they relate to Schroeder's paradox, which has been observed in Nafion.¹⁷ Briefly, Schroeder's paradox is the observation that for certain polymer membranes, water uptake is less when exposed to saturated water vapor than when exposed to liquid water, an apparent violation of thermodynamic equilibrium considerations. For the case of Nafion, several explanations have been proposed. Vallieres et al. found that a Flory-Huggins type model can produce a sorption isotherm that has multiple values for an activity of 1, analogous to a van der Waals loop.¹⁸ Onishi and Newman found that inconsistent thermal pretreatment of experimental samples can lead to varying water uptake at saturation, since experimental chains relax extremely slowly.¹⁹ Choi and Datta argued that at the membrane/vapor interface, exposed hydrophilic pores have a curved interface with the vapor, leading to an extra Laplace pressure on the pores that raises the chemical potential of water, thereby lowering the final water uptake²⁰ in comparison to a liquid-equilibrated membrane. Finally, Kusoglu et al.,²¹ as well as Benziger et al.,²² attribute the apparent difference in uptake to a difference in water sorption kinetics, specifically interfacial mass transfer resistance. This difference in resistance is thought to be a consequence of structural rearrangement of the polymer at the interfaces. Molec-

1
2
3 ular simulations of the interfaces could provide a molecular-level demonstration of this structural
4 rearrangement, complementing the body of experimental work^{12,13,21,23,24} that supports this ex-
5 planation for Schroeder's paradox.
6
7
8

9 Relatively few molecular simulations of the Nafion interfaces have been performed compared
10 to the number of bulk membrane studies. A study by Selvan et al of the Nafion/vapor interface²⁵
11 reported a region of water depletion near the vapor interface, in agreement with advancing contact
12 angle measurements that indicate that the interface is very hydrophobic.²⁴ The authors also studied
13 the orientation of hydronium near the interface, and found that the lone pair side of the molecule
14 tended to point towards the vapor phase, in agreement with previous simulations of hydrated pro-
15 tons at the liquid/vapor interface of water.²⁶ Additionally, the authors measured water diffusivities
16 parallel and perpendicular to the interface, and found that the diffusivities are *enhanced* relative to
17 the bulk. The authors concluded that "there is no observable additional resistance to mass transport
18 of the vehicular component of water and hydronium ions due to the interface." This intriguing con-
19 clusion appears to be at odds with experimental permeation studies showing that water transport
20 across the vapor interface is dramatically slower than across the bulk region.¹² One limitation of
21 the study was the membrane slab thickness: due to computational cost, the membrane slabs studied
22 by the authors were relatively thin (ca. 6 nm) compared to the length scale of the interface. More
23 recently, Borges et al. studied a slab of similar thickness, except with a solid surface of variable hy-
24 drophobicity on one side and vapor on the other.²⁷ Some of their findings were qualitatively similar
25 to those of Selvan et al.; for instance, they reported a hydrophobic, polymer-rich vapor interface.
26 However, they observed a modest slow-down of water dynamics instead of an enhancement as in
27 Selvan et al. In particular, they found that the diffusivity parallel to the interface decreased by *at*
28 *most* a factor of ca. 2 at the vapor interface, depending on the hydrophobicity of the solid surface.
29 Interestingly, this decrease in diffusivity is far smaller than the experimentally observed order-of-
30 magnitude difference in resistance between the interface and a macroscopically thick (ca. 100
31 μm) bulk region.¹² Other notable simulation studies of Nafion interfaces have focused on the in-
32 terface with the platinum catalyst^{28,29} or with the carbon support,³⁰ without attempting to compare
33
34
35
36
37
38
39
40
41
42
43
44
45
46
47
48
49
50
51
52
53
54
55
56
57
58
59
60

1
2
3
4
5
6
interfacial water transport to experiments.

7
8
9
10
11
12
13
14
15
16
17
18
19
20
21
22
23
24
25
26
27
28
29
30
31
32
33
Elucidation of the high mass transfer resistance at the vapor/membrane interface is the subject
of the present paper. This study also examines the liquid water/membrane interface, which has not
been addressed by past simulation studies to the best of our knowledge. The present work incorpo-
rates three methodological improvements relative to prior studies. In particular, the force-field used
has been verified to reproduce the experimental water sorption isotherm reasonably well,³¹ mak-
ing it suitable for studying interfacial mass transfer, which would depend heavily on differences in
solubility. The self-diffusivity of water is also accurately predicted by this force-field,³¹ although
in this regard the force-field is not unique.^{32,33} Another methodological improvement is the in-
creased thickness of the Nafion slabs, allowing the interfacial region to be clearly distinguished
from the bulk region. Finally, a recently developed non-equilibrium molecular dynamics (NEMD)
technique³⁴ was employed that produces transport properties that are more directly comparable
with experimental data than the diffusivity calculations reported in the past.^{25,27} The prior state-
of-the-art technique for studying interfacial mass transfer was dual control volume grand canonical
molecular dynamics,³⁵ which requires significant computational expense to converge.³⁶

34
35
36
37
38
39
40
41
42
43
44
45
46
47
48
49
In the present work, NEMD are performed on Nafion slabs in contact with vapor and liquid
water in order to calculate the resistance to water mass transfer at the interfaces. The molecular-
level structure of these interfaces is compared to the structure of bulk Nafion. The NEMD method
is also validated for a simple vapor/liquid system with known transport properties. Finally, the
interfacial resistance of the vapor interface of Nafion is compared to the resistance of crystalline
Teflon. The paper is organized as follows: the setup, execution, and analysis of the simulations
are described in Section 2; the results are discussed in Section 3, and the main conclusions are
summarized in Section 4.

2 Methods

2.1 Force field

Nafion consists of linear polytetrafluoroethylene (PTFE) chains attached to short, perfluoroether side-chains that each terminate with a sulfonic acid group.⁴ All CF_x groups were represented by united-atom sites without explicit fluorines for computational efficiency, while the rest of the atoms, including hydrogens, were modeled explicitly with point particles. The sulfonic acid groups were assumed to exist as covalently bound SO₃⁻ anions and mobile H₃O⁺ cations. H₃O⁺ cations were modeled classically with no delocalized excess proton, since proton conduction was not the emphasis of this work. Depending on the molecule, its constituent particles could interact through dispersion, coulombic, and bonded interactions; a full description of these interactions and their parameters can be found in Daly et al.³¹, which uses a modified version of the force-field from Cui et al.³⁷. CF_x parameters from this modified force-field were also used for C₆F₁₄ and C₉₆F₁₉₄ chains.

For Lennard-Jones interactions, an extra-long cut-off distance of 1.5 nm was used, since standard tail corrections cannot be simply applied to inhomogeneous systems. The electrostatic interactions were computed using the P3M Ewald summation method.³⁸ The interpolation order, grid-spacing, κ value, and real-space cut-off were set so that the rms error in the force on a particle was ca. 0.2 fN.³⁹

2.2 Setup and Equilibration

To accelerate equilibration of the Nafion chains, a low molecular weight of 3468 Da was chosen. Perfluoroether side-chains were spaced uniformly along the PTFE backbone as in Daly et al.³¹, since the placement of side-chains in experimental Nafion is unknown,⁴⁰ and is typically assumed to be uniform.⁴

The initial configurations were constructed by placing chains, waters, and hydroniums at random in rectangular boxes between 32 and 51 nm in length (*z* direction), with a square cross-

sectional area of 40 nm^2 . Particle positions that resulted in overlap between van der Waals radii were rejected. Argon atoms were also added so that the total pressure would be approximately 28 bar. This extra step was intended to lower the mean free path of molecules in the gas phase, thereby improving thermal equilibration of the system during the NEMD step. Note that at this pressure and a temperature of 353 K, argon is close to an ideal gas ($Z = 0.995^{41}$). In the Supporting Information, we show that raising the argon pressure has a negligible effect on the measured mass transfer resistance by conducting a duplicate vapor/Nafion run with a pressure of approximately 2.9 bar and obtaining essentially the same mass transfer resistance. The parameters for argon were 0.3345 nm for σ , and 125.7 K for ϵ .⁴²

The initial configurations were equilibrated using conventional NVT molecular dynamics, implemented in the HOOMD-blue simulation package,⁴³ at 1750 K for 0-10 ns, and finally quenched to 353 K. The temperature was fixed with the Nosé-Hoover thermostat.⁴⁴ The quenching caused the chains to spontaneously collapse into a slab that spanned the smaller two axes (xy) of the box. The slab was equilibrated for another 7.5-15 ns, with longer equilibration times used for systems at lower hydration. Finally, the coordinates of every particle in the system were translated so that the slab was in the center of the box ($z = 0$). Equilibrium densities of these systems in the bulk region ($z = 0$) are reported in the Supporting Information and compared to experiments.

The C_6F_{14} /vapor systems were equilibrated in the same way as the Nafion/vapor systems, while the $\text{C}_{96}\text{F}_{194}$ /vapor systems were not subjected to any high-temperature equilibration. Instead, the $\text{C}_{96}\text{F}_{194}$ /vapor systems were assembled by placing fully extended chains in a regular array in the center of the box, with the long chain axis parallel to the long box axis (see Supporting Information for details). The system was equilibrated for 75 ns, and the chains were shown to be in their equilibrium, crystalline configuration by calculating the $\text{CF}_2\text{-CF}_2$ pair correlation function in the bulk region. This pair correlation function was compared to that of a very long bulk MD simulation of $\text{C}_{96}\text{F}_{194}$ in which the chains spontaneously crystallize from the melt. Details of this comparison can be found in the Supporting Information.

The membrane/liquid-water systems were prepared using a protocol, explained in the follow-

1
2
3 ing paragraph, that prevented full dissolution of the membrane and allowed the system to reach
4 steady state. We would otherwise expect dissolution to occur based on previous calculations of the
5 sorption isotherm for low molecular weight systems,³¹ since it was found that even at very high
6 hydration ($\lambda \approx 30$, where λ denotes the number of water molecules per SO_3^- group), the activity of
7 water is still marginally less than 1, allowing further water uptake. We speculated that experimental
8 membranes would behave the same way, except that the high molecular weight and crystallinity of
9 the chains make the relevant timescales inaccessible.³¹ This hypothesis is supported by theoretical
10 models⁴⁵ as well as AFM experiments that show a nanoscopically rough interface,⁴⁶ consistent
11 with slowly dissolving chains.

12
13 Equilibrated configurations from the membrane/vapor simulations were used as a starting point
14 for preparing the membrane/liquid-water simulations. The chains were polymerized by using simu-
15 lated annealing⁴⁷ to identify a way of connecting the chain ends that would minimize the harmonic
16 bond potential energy. Then NVT molecular dynamics was performed for 2 ns while the spring
17 constants of newly formed bonds were gradually increased from 0 to the values prescribed by the
18 force-field. Next, the simulation box was elongated on each side of the slab and equilibrated liquid
19 water slabs were inserted in the newly added space, with enough room left over to ensure no over-
20 laps of van der Waals radii with existing particles in the system. The composite system was then
21 equilibrated for ca. 10 ns while keeping a subset of polymer backbone particles (CF_x 's) lying in a
22 prescribed control volume frozen to prevent full dissolution. These particles were frozen by sim-
23 ply switching off the NVT integrator for the entire subset. Once the system reached equilibrium, it
24 consisted of four phases: one membrane slab, two liquid slabs in contact with the membrane, and
25 one vapor phase connecting the two liquid slabs through the periodic boundary.

2.3 NEMD production runs

51
52 In order to simulate the permeation of water across the membrane interfaces and calculate relevant
53 transport properties, a recently developed non-equilibrium molecular dynamics (NEMD) method³⁴
54 was used. This method creates a steady-state chemical potential gradient and mass flux by impos-
55
56
57
58
59
60

1
2
3
4
5
6
7
8
9
10
11
12
13
14
15
16
17
18
19
20
21
22
23
24
25
26
27
28
29
30
31
32
33
34
35
36
37
38
39
40
41
ing an external force in the z direction, f_z , on permeant molecules (water) lying inside a control volume far away from the slab (see Figure 1). The placement of the control volume minimized simulation artifacts near the membrane interfaces. Additionally, the positions of the water molecules were updated using an NVE integrator to avoid artifacts introduced from thermostating. However, the remainder of the system was thermostatted using the Nosé-Hoover thermostat⁴⁴ in order to remove energy added to the system by the external force, thereby keeping the system at steady state. Periodic boundary conditions in all three dimensions were still used.

18
19
20
21
22
23
24
25
26
27
28
29
30
31
32
33
34
35
36
37
38
39
40
41
In its initial publication,³⁴ this NEMD method came in two varieties: single-current and counter-current. The single-current variant consists of applying the force in only the $+z$ direction, creating a net $+z$ flux, j_w , and overall $+z$ gradient in the chemical potential of water (see Figure 1). The counter-current variant adds an opposing $-z$ force in the same control volume, and applies the two opposing forces to two arbitrary halves of the total set of permeant molecules (water). This forcing scheme creates two opposing fluxes and two opposing chemical potential gradients, but no *overall* flux or chemical potential gradient. This second variant was chosen because it provides more information about the relative magnitudes of the interfacial and bulk resistances, as will be explained in Section 2.4. Unlike the single-current variant, the counter-current variant does not include pressure-driven mass transfer,³⁴ however we expect this type of mass transfer to be negligible experimentally, since both sides of the membrane are fixed at ca. 1 bar using dry or humidified N_2 ,¹² preventing any appreciable pressure gradient.

42
43
44
45
46
47
48
49
50
51
52
53
54
55
56
57
58
59
60

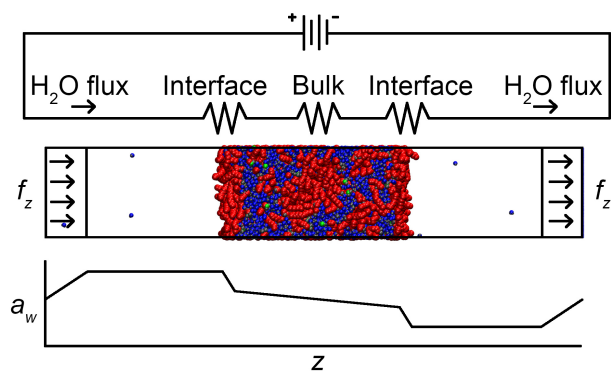


Figure 1: An external force applied in a control volume drives water mass transfer through a Nafion slab in contact with a vapor phase. The control volume is placed so that it is bisected by the z periodic boundary, as in Frentrup et al.³⁴. Top: schematic showing analogy with an electrical circuit. Middle: simulation box with the Nafion slab in the middle and the control volume far from the interface. Bottom: water activity profile as a function of z position in the box. Note that mass transfer in only one direction is shown for clarity; in the simulations, forces are applied in both directions to complementary sets of water molecules, creating countercurrent mass transfer.

2.4 Analysis

To compute an experimentally relevant mass transfer resistance, two quantities are needed from the simulation: the flux, j_w , and the activity gradient, Δa_w , for either subset of water molecules corresponding to the two opposing external forces. j_w was measured by counting the particle crossings at the periodic boundary, and dividing by the area and the elapsed time. In principle, particles crossings could be counted at any z coordinate, and a plot of $j_w(z)$ for one membrane/vapor system can be found in the Supporting Information. In practice, counting particle crossings in the vapor phase instead of the condensed phase resulted in much lower uncertainties for the flux.

Δa_w was measured by converting the particle concentrations in the vapor phases, measured just beyond the interfaces, to partial pressures using the ideal gas law. These partial pressures were then divided by the saturation pressure of water to obtain activities. The saturation pressure of water was measured independently with an NVT-MD simulation of a system of liquid water in contact with vapor at the same temperature and with the same Lennard-Jones cut-off. Once Δa_w and j_w are available, they can be combined using Eq. 1 to obtain a mass transfer resistance, R , for the entire

1
2
3 slab.
4
5
6

$$j_w = -\frac{\Delta a_w}{R} \quad (1)$$

7
8
9
10 Note that this method of obtaining R is identical to the experimental method.¹²
11
12

13 Care must be taken when defining the boundaries between the vapor phase and the condensed
14 phase, since these boundaries are where the activity drop is measured. For liquids and solids
15 consisting of linear perfluorocarbons, the boundaries were determined by first fitting the total mass
16 density profile perpendicular to the interface with a hyperbolic tangent function⁴⁸ (see Supporting
17 Information). The vapor interface was defined as the z coordinate at which the fitted profile equals
18 1.1 times the vapor concentration at $z = -\infty$. The vapor interface for Nafion systems proved more
19 ambiguous, since the mass density profile was non-monotonic and therefore could not be fit with a
20 hyperbolic tangent function (see Supporting Information). Instead, the vapor interface was defined
21 as the z coordinate at which the molar density equaled 0.045 g/cc, which was approximately 1.2
22 times the density at the z box edge. This threshold is large enough to exclude noise in the vapor
23 phase concentration profile, while still being small enough to exclude almost all of the condensed
24 phase.
25
26
27
28
29
30
31
32
33
34
35
36

37 If the *total*, uniform activity of water in the system is known, then the counter-current NEMD
38 method³⁴ can reveal not only the overall activity difference between the two sides of the condensed
39 phase *for a given subset of molecules*, but also the activity profile inside the condensed phase.
40
41 Consider the activity of subsets 1 and 2 at an arbitrary location z inside the simulation box:
42
43

$$a_1(z) = \frac{N_1(z)}{N_{tot}(z)} \gamma_1(z) \quad (2)$$

$$a_2(z) = \frac{N_2(z)}{N_{tot}(z)} \gamma_2(z) \quad (3)$$

54 $N_{tot}(z)$ is the total number of moles of all species at z . Note that $\gamma_1(z) = \gamma_2(z) = \gamma(z)$, since
55 molecules belonging to either subset are chemically identical. $\gamma(z)$ can be obtained from the activi-
56
57
58
59
60

ity of both subsets taken together:

$$\begin{aligned} a_{12} &= \frac{N_1(z) + N_2(z)}{N_{tot}(z)} \gamma(z) \\ &= \text{const} \end{aligned} \quad (4)$$

a_{12} can be easily computed by measuring the concentration in the vapor phase and applying the ideal gas law. Combining Eqs. 2-4, the activity of molecules belonging to subset 1 (or equivalently subset 2) at any point z inside the condensed phase can be expressed as follows:

$$a_1(z) = \frac{N_1(z)}{N_1(z) + N_2(z)} a_{12} \quad (5)$$

$a_1(z)$ was computed from simulation trajectories by dividing the box in the z direction into bins with thickness between $8 \cdot 10^{-3}$ and $12 \cdot 10^{-3}$ nm.

Nafion side chains near the interface may experience some degree orientational order that can be quantified using the nematic order parameter:⁴⁹

$$S_2 = \frac{1}{N} \left\langle \sum_{i=1}^N \frac{3}{2} (\mathbf{u}_i \cdot \mathbf{n})^2 - \frac{1}{2} \right\rangle \quad (6)$$

where \mathbf{u}_i is a unit vector parallel to the displacement vector between the coordinates of the sulfur and the backbone carbon belonging to side-chain i . \mathbf{n} is the average orientation of the side-chain given by the eigenvector corresponding to the largest eigenvalue of the orientation tensor $\langle \mathbf{Q} \rangle$ ⁴⁹. $S_2 = 1$ represents perfectly aligned side-chains, whereas $S_2 = 0$ represents randomly aligned side-chains.

3 Results and Discussion

3.1 Method validation: C₆F₁₄ vapor/liquid

The NEMD method of Frentrup et al.³⁴ was initially demonstrated on a system of a Lennard-Jones liquid flowing through a rigid slit pore. The Nafion systems of interest are amorphous solids and liquids in contact with a vapor phase. Because of this difference, the NEMD method was first tested on a simple system consisting of a C₆F₁₄ liquid slab in contact with a vapor. This system bears a much closer resemblance to the Nafion systems than the original slit pore system. In the Supporting Information, the mass transfer resistance of this system is measured directly and compared to an estimate obtained by combining the transport diffusivity, activity coefficient, concentration, and slab thickness. The transport diffusivity is also compared to the self-diffusivity of water from EMD. These comparisons are performed over a range of different values of the external force to demonstrate the robustness of the NEMD method for these types of systems.

3.2 Nafion: membrane/vapor interface

Membrane/vapor systems were prepared with three different membrane thicknesses and studied at two different humidities, as summarized in Table 1. All systems were subjected to an external body force, f_z , of 4.98 pN applied in a control volume defined approximately 10 nm from the interface. An external force of this magnitude was chosen because it was found in the Supporting Information to be a good compromise between accuracy and precision. For each state point, statistical uncertainties were obtained from multiple runs initialized with uncorrelated configurations. The average concentration profile of one such state point is shown in Figure 2. Within the first nm of the vapor interface, there is an enrichment of hydrophobic CF_x groups that form the polymer backbone and side-chain, in qualitative agreement with earlier simulation work,^{25,27} as well as advancing contact angle experiments.²⁴ The peak in CF_x concentration is followed by a peak in sulfur concentration, which overlaps with a peak in water concentration. This last peak ends at approximately 5 nm from the vapor interface, after which all three species reach their bulk

concentrations ($\rho / \rho_{bulk} \rightarrow 1$). Cross-sectional slices parallel to the interface are shown in Figure 3 (top) from both the bulk region ($z \gtrsim -9$ nm) and the interfacial region ($z \lesssim -9$ nm). At the vapor interface, the CF_x species form a continuous hydrophobic layer with no hydrophilic clusters. Near the interface, the side chains appears to preferentially orient themselves toward the interior of the membrane, as shown in Figure 3 (bottom). This orientational order can be quantified with the property S_2 , which sharply increases from 0 to 1 at $-7 < z < 5$ nm, as seen in Figure 4. The orientational order disappears after only a 2 nm separation from the vapor interface. When water is removed from the system, the hydrophobic layer at the interface remains, but is not as enriched with CF_x compared to the bulk region, as shown in the Supporting Information. This difference is not surprising considering that the density of CF_x groups anywhere inside the membrane will increase when water is removed.

Table 1: Membrane thickness, overall water activity, and resistance to water mass transfer ($-\Delta a_w / j_w$) as a function of composition of vapor/membrane systems. Uncertainties in the smallest significant figure are reported in parentheses.

# chains	#H ₂ O & H ₃ O ⁺	l_z (nm)	a_w	$R(\text{cm}^2 \cdot \text{min/mol})$
64	3082	8.25(2)	0.86(6)	1.1(2)
64	384	6.34(6)	0.12(2)	1.6(2)
128	6164	14.48(3)	0.87(4)	1.3(2)
256	12328	27.10(3)	0.85(7)	1.6(4)
256	1536	19.69(8)	0.14(2)	2.2(7)

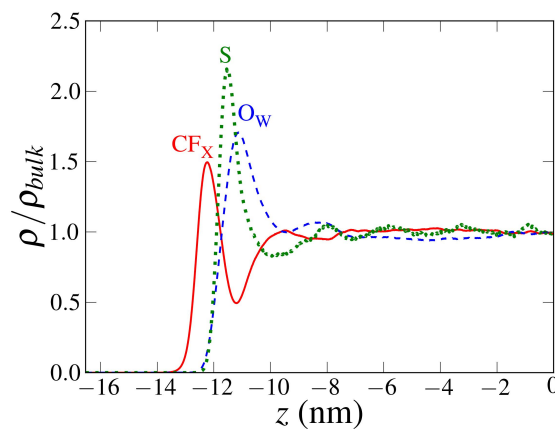


Figure 2: Densities of different species as a function of distance from the center of the Nafion slab for systems with 256 chains and 12328 water molecules ($a_w = 0.85 \pm 0.07$). “ CF_X ” refers to CF_3 , CF_2 , and CF groups; “S” refers to just sulfur atoms; “ O_W ” refers to oxygens belonging to either H_2O or H_3O^+ . Densities are normalized by their values from simulations of bulk Nafions at $\lambda = 16.1$, $T = 353$ K, and $p = 1$ bar.

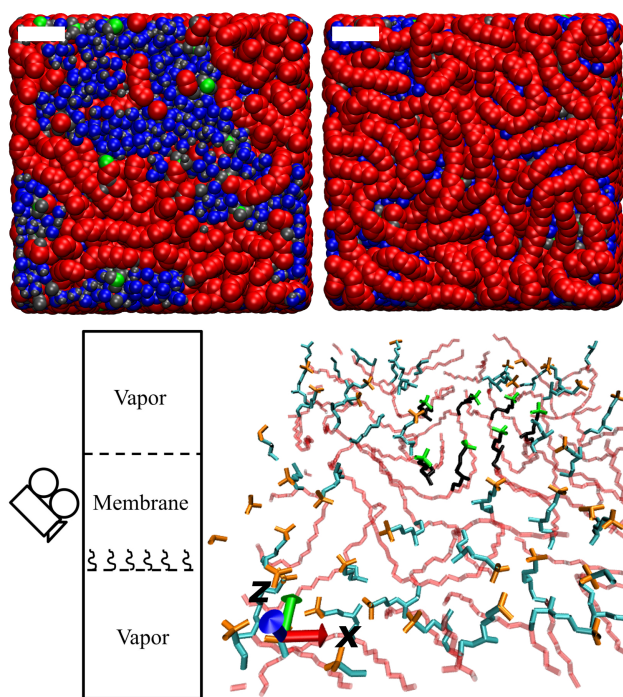


Figure 3: Top: cross-section of the Nafion membrane perpendicular to the z axis for systems with 256 chains and 12328 water molecules (H_2O and H_3O^+). Color coding is the same as in Figure 2, with the addition of gray particles that represent hydrogens, perfluoroether oxygens, and sulfonate oxygens. White scale bars denote lengths of 1 nm. Top left: cross-section in the bulk region of the slab ($1 > z > -2$, where $z = 0$ is the center of the slab). Top right: cross-section in the interfacial region of the slab ($-11 > z > -14$). Bottom: snapshot of polymer side-chains aligned toward the interior of the membrane for a system consisting of 128 chains and 6164 water molecules (H_2O and H_3O^+) in contact with a vapor phase (see diagram on left-hand side). Side-chains with $-7 < z < -4.8$ are visible, with cyan and orange portions corresponding to perfluoroether and SO_3^- , respectively. A few side-chains are colored in black and green, respectively, to make their orientations more clear. Polymer backbone is shown in red.

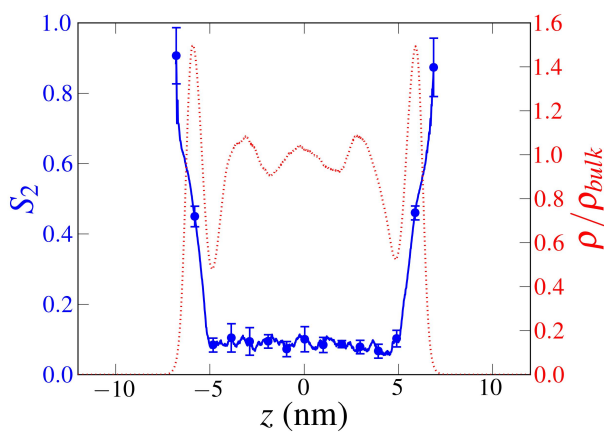


Figure 4: Alignment of the polymer side chains in a Nafion/vapor system consisting of 128 chains and 6164 water molecules (H_2O and H_3O^+). Blue curve: orientational order parameter, S_2 . $S_2 = 1$ represents perfect alignment, whereas $S_2 = 0$ represents random alignment. Error bars are shown at regular intervals. Red dotted curve: number density of CF_x species normalized by their density from simulations of bulk Nafions at $\lambda = 16.1$.

As water moves from a high activity interface of the membrane to a low activity interface, most of the activity drop occurs within the 1-nm thick hydrophobic layer at the interface, as shown in Figure 5. This sharp drop in activity corresponds to a high interfacial transport resistance, as confirmed by the cumulative mass transfer resistance, $R(z)$, plotted in Figure 6. The curves in this figure demonstrate that the cumulative resistance sharply increases at the interfaces, while remaining relatively constant in the bulk region. A related quantity is the *local* resistance, $r(z)$, which is defined and plotted in the Supporting Information. Note that $R(z)$ for the systems of different thickness have the same slopes, to within the statistical uncertainty, for both the interfacial and bulk regions, indicating the absence of strong finite size effects. The very large observed difference between interfacial and bulk resistances in Figure 6 is not seen in small molecule liquids with negligible amphiphilic character. For example, $R(z)$ for a C_6F_{14} vapor/liquid system does not exhibit any sharp increase at the interfaces, as seen in Figure S8 in the Supporting Information.

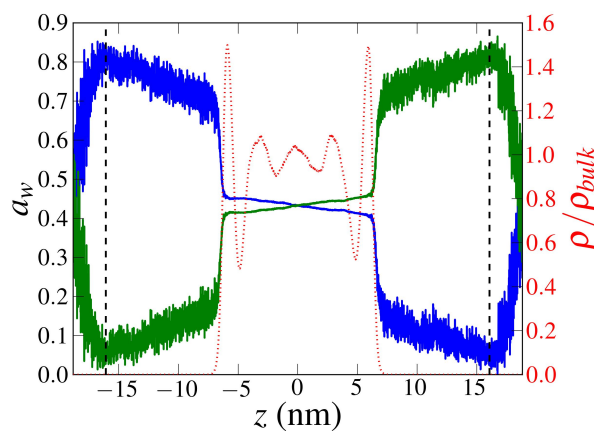


Figure 5: Water activity profile, $a_w(z)$, across a Nafion slab with 128 chains and 6164 water molecules (H_2O and H_3O^+) in contact with a vapor phase at $T = 353$ K and $p \approx 28$ bar. $a_w(z)$ for a given subset of water molecules is computed using Eq. 5. Blue curve: activity of molecules forced in the $+z$ direction. Green curve: activity of molecules forced in the $-z$ direction. Red dotted curve: number density of CF_x species normalized by their density from simulations of bulk Nafion at $\lambda = 16.1$. Black dashed lines: boundaries of the control volume in which the external force is applied.

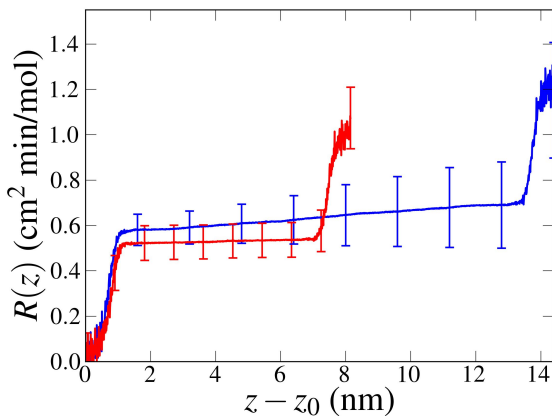


Figure 6: Cumulative resistance, $R(z) = [a_w(z) - a_w(z_0)]/j_w$, as a function of distance across the Nafion slab, moving from one interface ($z = z_0$) to the other. Red curve: system with 64 chains and 3082 waters (H_2O and H_3O^+). Blue curve: system with 128 chains and 6164 waters. Error bars for the curves are shown at regular intervals.

Figure 7 quantitatively compares the bulk and interfacial resistances of a Nafion membrane in contact with a vapor phase. The interfacial resistance is taken to be the resistance accumulated in the first or last 1 nm of the blue curve in Figure 6. The remaining accumulated resistance

($\sim 0.1 \text{ cm}^2 \text{min/mol}$) makes up the bulk resistance. In Figure 7, the bulk resistance is normalized by the length of the bulk region ($\sim 12 \text{ nm}$) in Figure 6. Figure 7 shows that there is a nearly two order of magnitude difference between the bulk and interfacial resistances, in qualitative agreement with permeation experiments.¹² However, the interfacial resistance from simulations is still nearly three orders of magnitude smaller than the value from permeation experiments. Reasons for this difference will be proposed in the discussion that follows.

Simulations show that the vapor interface consists of a 1 nm thick Teflon-like layer (see Figure 2 and top of Figure 3), so a natural comparison to make is with experimental permeation measurements on pure Teflon.⁵⁰ These measurements were demonstrated to be extremely sensitive to the density of the Teflon sample, which is in turn related to the degree of crystallinity. A full plot of experimental permeation data over a wide range of densities can be found in the Supporting Information. In Figure 7, the upper and lower bounds of available experimental data for Teflon are included. The interfacial resistance of Nafion from simulations falls within these bounds, as does the resistance of Nafion from experiments, although this resistance lies much closer to the upper bound.

Also included in Figure 7 is the resistance of a purely crystalline slab of Teflon measured using simulations. Details of these simulations can be found in Section 2.2 and the Supporting Information. The resistance from these crystalline slabs is one order of magnitude less than the upper bound of experimental Teflon data. At present it is unknown whether this discrepancy can be attributed to force-field inaccuracy, since the error bars and exact amount of crystallinity in the experimental Teflon data from Hadge et al.⁵⁰ is unknown. On the other hand, the resistance from the Teflon simulations is within one order of magnitude of the experimental Nafion data, demonstrating that the perfluoroalkane force-field is capable of producing the very high resistances. Therefore, we speculate that force-field error is not the most important factor responsible for the differences seen between simulated Nafion and experimental Nafion.

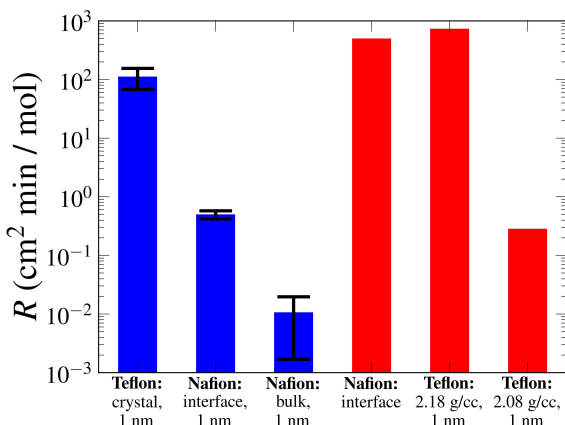


Figure 7: Mass transfer resistance, R , measured from simulations (blue) and experiments (red) at 353 K. All resistances correspond to a 1 nm thick slab of material except for the experimental resistance for the vapor/Nafion interface,¹² which has an unknown thickness. The different densities of experimental samples of Teflon reflect different degrees of crystallinity achieved by molding the material at different pressures.⁵⁰

In light of the comparison with Teflon data in Figure 7, we speculate that polymer crystallinity at the interface may be an important factor responsible for the extremely high mass transfer resistance of experimental samples. This would not be surprising considering that the experimental melting point of pure Teflon is nearly 300 K higher than the temperature at which simulations and experiments are performed, 353 K. In addition, GISAXS experiments on spin-coated Nafion films show changes in the scattering near the surface that are analogous to changes seen in bulk samples after stretching.⁴⁶ The authors interpreted this observation as in-plane alignment of the Teflon-like backbone at the vapor interface.

In the simulations, the interface of Nafion appears very amorphous (see top of Figure 3). The degree of crystallinity was quantified by plotting S_2 as a function of z for polymer backbone segments consisting of 16 CF_x groups. Plots for vapor/membrane and vapor/Teflon systems can be found in the Supporting Information. For a crystalline system like Teflon, $S_2 \approx 1$, whereas the amorphous vapor interface seen in Figure 3 (top) has $S_2 \approx 0.3$.

It's plausible that crystallinity can only be achieved by simulating with very high MW chains and/or over very long time scales that are inaccessible with current computing power. This limi-

tation may partially explain the very modest differences in water dynamics between the bulk and interfacial regions observed in prior simulations.^{25,27} Nevertheless, even with an amorphous interface, a huge difference between interfacial and bulk resistance was observed in our simulations.

3.3 Nafion: membrane/liquid water interface

A steady-state configuration from a vapor/liquid-water/membrane simulation can be seen in Figure 8 with four distinct phases: a membrane phase in the middle, two liquid water phases that bound the membrane phase, and a vapor phase. Figure 8 also highlights a subset of backbone CF_x groups in the center of the membrane that are immobilized, as described in Section 2.2. In the Supporting Information, membrane/vapor interface systems with immobilization and no immobilization are compared as a test of the method. It is shown that immobilizing the backbone has a negligible impact on the mass transfer resistance.

The remaining chain segments appear to be highly swollen with water to the extent that their sulfonate groups are in contact with the liquid water phase. This nanoscopically rough interface is consistent with AFM experiments showing nanoscale peaks and valleys not present at the vapor interface.²³ The observed swollen chains are also qualitatively similar to the highly solvated chain configurations observed in recent scattering experiments with dilute solutions of Nafion in water/2-propanol mixtures.⁵¹ The exposed sulfonate groups suggest a very hydrophilic interface, in agreement with receding contact angle experiments.²⁴ The concentration of sulfonate groups, CF_x groups, and water molecules are presented in Figure 9 as a function of distance from the center of the membrane. Interestingly, there is a more or less linear decrease in polymer concentration with increasing separation from the immobilized region of the membrane.

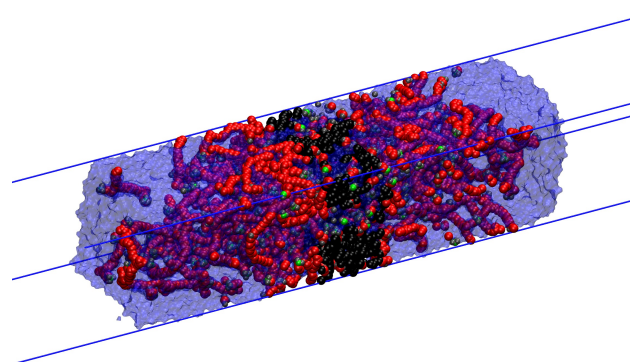


Figure 8: Snapshot of a vapor/liquid water/membrane system with one 441600 Da chain and 23504 water molecules (H_2O and H_3O^+). Color coding is the same as in Figure 2, with the exception of backbone CF_x groups that fall within the “frozen” region ($-2 < z < 2 \text{ nm}$), which are colored black. In addition, oxygens belonging to H_2O and H_3O^+ are represented with a semi-transparent Connolly surface⁵² instead of explicit spheres for clarity.

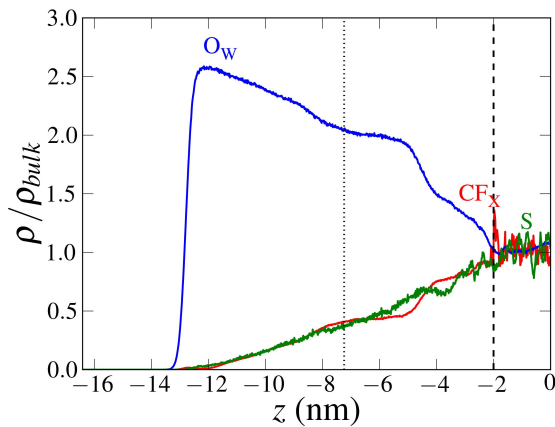


Figure 9: Densities of different species as a function of distance from the center of the liquid/membrane slab for vapor/liquid water/membrane systems with one 441600 Da chain and 23504 water molecules (H_2O and H_3O^+). Labels for individual curves are the same as in Figure 2. Densities are normalized by their values from simulations of bulk Nafion at $\lambda = 16.1$, $T = 353 \text{ K}$, and $p = 1 \text{ bar}$. Dashed line marks the boundary of the region in which backbone CF_X groups are frozen. Dotted line marks the approximate location of the vapor interface for the system in Figure 5, which was used for the membrane initial configuration, as described in Section 2.2.

The water activity profiles for the vapor/liquid water/membrane system are shown in Figure 10. The shape of these profiles is the opposite of what was observed in Figure 5: the steepest drop in activity occurs at the center of the membranes, while the slope of activity at the liquid water/vapor

interfaces is nearly flat. The shape of the activity profile suggests that the majority of the mass transfer resistance occurs in the bulk region, while the resistance at the liquid water interface is negligible, in agreement with permeation experiments.¹²

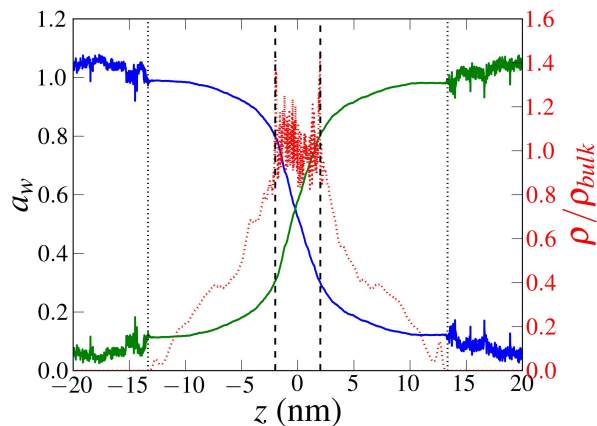


Figure 10: Water activity profile, $a_w(z)$, in a vapor/liquid water/Nafion system with one 441600 Da chain and 23504 water molecules. $a_w(z)$ for a given subset of water molecules is computed using Eq. 5. Blue curve: activity of molecules forced in the $+z$ direction. Green curve: activity of molecules forced in the $-z$ direction. Red dotted curve: number density of CF_x species normalized by their density from simulations of bulk Nafion at $\lambda = 16.1$. Black dashed line: the boundary of the region in which backbone CF_X groups are frozen. Black dotted lines: the vapor/liquid water interfaces.

4 Conclusions

NEMD was performed on Nafion membranes in contact with liquid water and water vapor near saturation in order to measure interfacial water mass transfer resistances and determine their molecular origins. Near the vapor interface, low-MW Nafion chains form a 1 nm thick, amorphous, hydrophobic layer with sulfonate groups oriented towards the interior of the membrane. This hydrophobic layer completely covers the hydrophilic pores in the bulk region of the membrane, contradicting a previous hypothesis of exposed pores.²⁰ The mass transfer resistance of this hydrophobic layer is comparable to that of low-density Teflon. This resistance is nearly two orders of magnitude greater than the resistance of bulk membrane material, in qualitative agreement with permeation experiments. However, the experimental mass transfer resistance of the vapor interface

is closer to that of high-density, highly crystalline Teflon, and much higher than the resistances obtained from our simulations of amorphous samples. In light of this observation as well as GISAXS measurements of nafion films in contact with water vapor,²³ we speculate that surface crystallinity of the polymer may play a significant role in impeding water mass transfer across the membrane.

When Nafion is placed in contact with liquid water, the chains near the interface extend into the liquid water phase, exposing their sulfonate groups to bulk water and forming a hydrophilic interface. These highly swollen chain configurations appear to be consistent with AFM experiments²³ as well scattering experiments on Nafion in dilute water/2-propanol solutions.⁵¹ Moreover, the mass transfer resistance at the liquid-water interface is negligible compared to that of bulk membrane material, in qualitative agreement with permeation experiments.

More broadly, this work studies a polymer membrane in contact with a solvent in two different phases with nearly the same activity; it is shown that the phase of the solvent profoundly affects the structure and transport properties at the interface. This behavior is not commonplace, since it is a direct consequence of the amphiphilic chemistry of Nafion, which permits hydrophobic segments to concentrate at the vapor interface to form a region with drastically different water solubility than the bulk. This behavior is also consistent with the mass-transfer hypothesis for Schroeder's Paradox, in which the interfacial resistance reduces the apparent water uptake of vapor-equilibrated Nafion relative to liquid-equilibrated Nafion.^{21,22} The high MW of the chains prevents the membrane from reaching its true equilibrium state on experimental times scales.

The practical implication of this work is that ionomer backbone chemistry is critical for interfacial water mass transfer. The extremely hydrophobic teflon backbone in Nafion is responsible for the very high mass transfer resistance at the vapor interface, an attractive property for fuel cell operation. Less hydrophobic backbones such as polyethylene (found in sulfonated polystyrene⁵³) or polyether ether ketone (found in sulfonated polyether ether ketone⁵⁴) would be expected to have lower mass transfer resistances at the vapor interface. Permeation experiments on these ionomers can be used to test this hypothesis.

Acknowledgements

P. G. D. gratefully acknowledges the support of the National Science Foundation (Grant No. CHE-1213343). A. Z. P. would like to acknowledge support for this work from the Department of Energy, Office of Basic Energy Sciences, under grant DE-SC0002128.

Supporting Information Available: validation of the NEMD method, including tests with C₆F₁₄; details of the initial configuration of the Teflon system; experimental reference data for Teflon; mass density profiles and data for Nafion; results for Nafion at low humidity; crystallinity data. This material is available free of charge via the Internet at <http://pubs.acs.org>.

References

- (1) Geise, G. M.; Lee, H.-S.; Miller, D. J.; Freeman, B. D.; McGrath, J. E.; Paul, D. R. Water Purification by Membranes: The Role of Polymer Science. *Journal of Polymer Science Part B: Polymer Physics* **2010**, *48*, 1685–1718.
- (2) O'Brien, T. F.; Bommaraju, T. V.; Hine, F. *Handbook of Chlor-Alkali Technology: Volume I: Fundamentals*; Springer, 2007.
- (3) Zaidi, J.; Matsuura, T. *Polymer Membranes for Fuel Cells*; Springer, 2010.
- (4) Mauritz, K. A.; Moore, R. B. State of Understanding of Nafion. *Chemical Reviews* **2004**, *104*, 4535–4586.
- (5) Yang, C.; Srinivasan, S.; Bocarsly, A. B.; Tulyani, S.; Benziger, J. B. A Comparison of Physical Properties and Fuel Cell Performance of Nafion and Zirconium Phosphate/Nafion Composite Membranes. *Journal of Membrane Science* **2004**, *237*, 145–161.
- (6) Naudy, S.; Collette, F.; Thominette, F.; Gebel, G.; Espuche, E. Influence of Hygrothermal Aging on the Gas and Water Transport Properties of Nafion® Membranes. *Journal of Membrane Science* **2014**, *451*, 293–304.

- 1
2
3 (7) Modestino, M. A.; Paul, D. K.; Dishari, S.; Petrina, S. A.; Allen, F. I.; Hickner, M. A.;
4 Karan, K.; Segalman, R. A.; Weber, A. Z. Self-Assembly and Transport Limitations in Con-
5 fined Nafion Films. *Macromolecules* **2013**, *46*, 867–873.
6
7
8 (8) Hwang, G. S.; Parkinson, D. Y.; Kusoglu, A.; MacDowell, A. A.; Weber, A. Z. Understanding
9 Water Uptake and Transport in Nafion Using X-Ray Microtomography. *ACS Macro Lett.*
10 **2013**, *2*, 288–291.
11
12
13 (9) Kreuer, K.-D.; Portale, G. A Critical Revision of the Nano-Morphology of Proton Conducting
14 Ionomers and Polyelectrolytes for Fuel Cell Applications. *Advanced Functional Materials*
15 **2013**, *23*, 5390–5397.
16
17 (10) Benziger, J. Fan the Flame With Water: Current Ignition, Front Propagation and Multi-
18 ple Steady States in Polymer Electrolyte Membrane Fuel Cells. *AICHE Journal* **2009**, *55*,
19 3034–3040.
20
21
22 (11) Hogarth, W. H.; Benziger, J. B. Operation of Polymer Electrolyte Membrane Fuel Cells With
23 Dry Feeds: Design and Operating Strategies. *Journal of Power Sources* **2006**, *159*, 968–978.
24
25
26 (12) Majsztrik, P.; Bocarsly, A.; Benziger, J. Water Permeation Through Nafion Membranes: The
27 Role of Water Activity. *J. Phys. Chem. B* **2008**, *112*, 16280–16289.
28
29
30 (13) Adachi, M.; Navessin, T.; Xie, Z.; Li, F. H.; Tanaka, S.; Holdcroft, S. Thickness Dependence
31 of Water Permeation Through Proton Exchange Membranes. *Journal of Membrane Science*
32 **2010**, *364*, 183–193.
33
34
35 (14) Romero, T.; Mérida, W. Water Transport in Liquid and Vapour Equilibrated NafionTM Mem-
36 branes. *Journal of Membrane Science* **2009**, *338*, 135–144.
37
38
39 (15) Zhang, Z.; Martin, J.; Wu, J.; Wang, H.; Promislow, K.; Balcom, B. J. Magnetic Resonance
40 Imaging of Water Content Across the Nafion Membrane in an Operational PEM Fuel Cell.
41 *Journal of Magnetic Resonance* **2008**, *193*, 259–266.
42
43
44
45
46
47
48
49
50
51
52
53
54
55
56
57
58
59
60

- (16) Pivovar, B. S.; Kim, Y. S. The Membrane–Electrode Interface in PEFCs I. A Method for Quantifying Membrane–Electrode Interfacial Resistance. *J. Electrochem. Soc.* **2007**, *154*, B739–B744.
- (17) Zawodzinski, T. A.; Springer, T. E.; Davey, J.; Jestel, R.; Lopez, C.; Valerio, J.; Gottesfeld, S. A Comparative Study of Water Uptake by and Transport Through Ionomeric Fuel Cell Membranes. *J. Electrochem. Soc.* **1993**, *140*, 1981–1985.
- (18) Vallieres, C.; Winkelmann, D.; Roizard, D.; Favre, E.; Scharfer, P.; Kind, M. On Schroeder’s Paradox. *Journal of Membrane Science* **2006**, *278*, 357–364.
- (19) Onishi, L. M.; Prausnitz, J. M.; Newman, J. Water–Nafion Equilibria. Absence of Schroeder’s Paradox. *The Journal of Physical Chemistry B* **2007**, *111*, 10166–10173.
- (20) Choi, P.; Datta, R. Sorption in Proton-Exchange Membranes an Explanation of Schroeder’s Paradox. *J. Electrochem. Soc.* **2003**, *150*, E601–E607.
- (21) Kusoglu, A.; Modestino, M. A.; Hexemer, A.; Segalman, R. A.; Weber, A. Z. Subsecond Morphological Changes in Nafion During Water Uptake Detected by Small-Angle X-Ray Scattering. *ACS Macro Lett.* **2012**, *1*, 33–36.
- (22) Benziger, J.; Bocarsly, A.; Cheah, M. J.; Majsztrik, P.; Satterfield, B.; Zhao, Q. Mechanical and Transport Properties of Nafion: Effects of Temperature and Water Activity. In *Fuel Cells and Hydrogen Storage*; Bocarsly, A., Mingos, D. M. P., Eds.; Structure and Bonding 141; Springer Berlin Heidelberg, 2011; pp 85–113.
- (23) Bass, M.; Berman, A.; Singh, A.; Konovalov, O.; Freger, V. Surface Structure of Nafion in Vapor and Liquid. *J. Phys. Chem. B* **2010**, *114*, 3784–3790.
- (24) Goswami, S.; Klaus, S.; Benziger, J. Wetting and Absorption of Water Drops on Nafion Films. *Langmuir* **2008**, *24*, 8627–8633.

- 1
2
3 (25) Selvan, M. E.; Liu, J.; Keffer, D. J.; Cui, S.; Edwards, B. J.; Steele, W. V. Molecular Dyna-
4 mics Study of Structure and Transport of Water and Hydronium Ions at the Membrane/Vapor
5 Interface of Nafion. *The Journal of Physical Chemistry C* **2008**, *112*, 1975–1984.
6
7
8
9
10 (26) Petersen, M. K.; Iyengar, S. S.; Day, T. J. F.; Voth, G. A. The Hydrated Proton at the Water
11 Liquid/Vapor Interface. *J. Phys. Chem. B* **2004**, *108*, 14804–14806.
12
13
14 (27) Damasceno Borges, D.; Franco, A. A.; Malek, K.; Gebel, G.; Mossa, S. Inhomogeneous
15 Transport in Model Hydrated Polymer Electrolyte Supported Ultrathin Films. *ACS Nano*
16 **2013**, *7*, 6767–6773.
17
18
19
20
21
22 (28) Selvan, M. E.; He, Q.; Calvo-Muñoz, E. M.; Keffer, D. J. Molecular Dynamic Simulations
23 of the Effect on the Hydration of Nafion in the Presence of a Platinum Nanoparticle. *J. Phys.*
24
25
26
27
28
29 (29) Liu, J.; Selvan, M. E.; Cui, S.; Edwards, B. J.; Keffer, D. J.; Steele, W. V. Molecular-Level
30 Modeling of the Structure and Wetting of Electrode/Electrolyte Interfaces in Hydrogen Fuel
31 Cells. *J. Phys. Chem. C* **2008**, *112*, 1985–1993.
32
33
34
35
36 (30) Mashio, T.; Malek, K.; Eikerling, M.; Ohma, A.; Kanesaka, H.; Shinohara, K. Molecular
37 Dynamics Study of Ionomer and Water Adsorption at Carbon Support Materials. *J. Phys.*
38
39
40
41
42
43
44 (31) Daly, K. B.; Benziger, J. B.; Debenedetti, P. G.; Panagiotopoulos, A. Z. Molecular Dynamics
45 Simulations of Water Sorption in a Perfluorosulfonic Acid Membrane. *J Phys Chem B* **2013**,
46 *117*, 12649–12660.
47
48
49
50
51 (32) Tse, Y.-L. S.; Herring, A. M.; Kim, K.; Voth, G. A. Molecular Dynamics Simulations of
52 Proton Transport in 3M and Nafion Perfluorosulfonic Acid Membranes. *J. Phys. Chem. C*
53 **2013**, *117*, 8079–8091.
54
55
56
57
58
59
60

- (33) Devanathan, R.; Venkatnathan, A.; Dupuis, M. Atomistic Simulation of Nafion Membrane: I. Effect of Hydration on Membrane Nanostructure. *The Journal of Physical Chemistry B* **2007**, *111*, 8069–8079.
- (34) Frentrup, H.; Avendaño, C.; Horsch, M.; Salih, A.; Müller, E. A. Transport Diffusivities of Fluids in Nanopores by Non-Equilibrium Molecular Dynamics Simulation. *Molecular Simulation* **2012**, *38*, 540–553.
- (35) Cracknell, R. F.; Nicholson, D.; Quirke, N. Direct Molecular Dynamics Simulation of Flow Down a Chemical Potential Gradient in a Slit-Shaped Micropore. *Phys. Rev. Lett.* **1995**, *74*, 2463–2466.
- (36) Arya, G.; Chang, H.-C.; Maginn, E. J. A Critical Comparison of Equilibrium, Non-Equilibrium and Boundary-Driven Molecular Dynamics Techniques for Studying Transport in Microporous Materials. *The Journal of Chemical Physics* **2001**, *115*, 8112–8124.
- (37) Cui, S.; Liu, J.; Selvan, M. E.; Keffer, D. J.; Edwards, B. J.; Steele, W. V. A Molecular Dynamics Study of a Nafion Polyelectrolyte Membrane and the Aqueous Phase Structure for Proton Transport. *The Journal of Physical Chemistry B* **2007**, *111*, 2208–2218.
- (38) Hockney, R.; Eastwood, J. *Computer Simulation Using Particles*; Institute of Physics, 1992.
- (39) Deserno, M.; Holm, C. How to Mesh Up Ewald Sums. II. an Accurate Error Estimate for the Particle-particle-particle-Mesh Algorithm. *J. Chem. Phys.* **1998**, *109*, 7694.
- (40) Jang, S. S.; Molinero, V.; Çagin, T.; Goddard III, W. A. Effect of Monomeric Sequence on Nanostructure and Water Dynamics in Nafion 117. *Solid State Ionics* **2004**, *175*, 805–808.
- (41) Linstrom, P. J.; Mallard, W. G. *NIST Chemistry WebBook, NIST Standard Reference Database Number 69*; National Institute of Standards and Technology, Gaithersburg MD, 20899, 2014.
- (42) White, J. A. Lennard-Jones as a Model for Argon and Test of Extended Renormalization Group Calculations. *The Journal of chemical physics* **1999**, *111*, 9352.

- 1
2
3 (43) Anderson, J. A.; Lorenz, C. D.; Travesset, A. General Purpose Molecular Dynamics Simu-
4
5
6
7
8
9
10
11
12
13
14
15
16
17
18
19
20
21
22
23
24
25
26
27
28
29
30
31
32
33
34
35
36
37
38
39
40
41
42
43
44
45
46
47
48
49
50
51
52
53
54
55
56
57
58
59
60 (43) Anderson, J. A.; Lorenz, C. D.; Travesset, A. General Purpose Molecular Dynamics Simulations Fully Implemented on Graphics Processing Units. *Journal of Computational Physics* **2008**, 227, 5342–5359.
- (44) Nosé, S. A Unified Formulation of the Constant Temperature Molecular Dynamics Methods. *The Journal of Chemical Physics* **1984**, 81, 511.
- (45) Freger, V. Hydration of Ionomers and Schroeder's Paradox in Nafion. *J. Phys. Chem. B* **2009**, 113, 24–36.
- (46) Bass, M.; Berman, A.; Singh, A.; Konovalov, O.; Freger, V. Surface Structure of Nafion in Vapor and Liquid. *J. Phys. Chem. B* **2010**, 114, 3784–3790.
- (47) Press, W. H.; Teukolsky, S. A.; Vetterling, W. T.; Flannery, B. P. *Numerical Recipes 3rd Edition: The Art of Scientific Computing*, 3rd ed.; Cambridge University Press, 2007.
- (48) Widom, B. Potential-Distribution Theory and the Statistical Mechanics of Fluids. *The Journal of Physical Chemistry* **1982**, 86, 869–872.
- (49) Eppenga, R.; Frenkel, D. Monte Carlo Study of the Isotropic and Nematic Phases of Infinitely Thin Hard Platelets. *Molecular physics* **1984**, 52, 1303–1334.
- (50) Hadge, R. G.; Riddell, Malcolm N.; O'Toole, John L., Quick Vapor Permeability Test for Molded Plastics. *SPE J.* **1972**, 28, 58–63.
- (51) Welch, C.; Labouriau, A.; Hjelm, R.; Orler, B.; Johnston, C.; Kim, Y. S. Nafion in Dilute Solvent Systems: Dispersion or Solution? *ACS Macro Lett.* **2012**, 1, 1403–1407.
- (52) Connolly, M. L. Analytical Molecular Surface Calculation. *Journal of Applied Crystallography* **1983**, 16, 548–558.
- (53) Mauritz, K. A. Review and Critical Analyses of Theories of Aggregation in Ionomers. *Journal of Macromolecular Science, Part C: Polymer Reviews* **1988**, 28, 65–98.

- (54) Liu, B.; Robertson, G. P.; Kim, D.-S.; Guiver, M. D.; Hu, W.; Jiang, Z. Aromatic Poly(ether Ketone)s With Pendant Sulfonic Acid Phenyl Groups Prepared by a Mild Sulfonation Method for Proton Exchange Membranes. *Macromolecules* **2007**, *40*, 1934–1944.

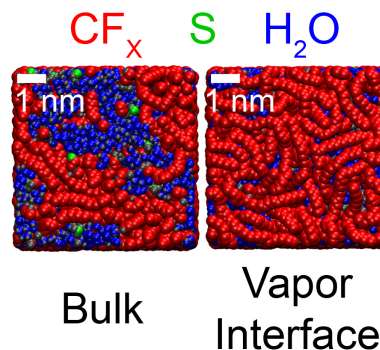


Figure 11: Table of Contents Image